Regimes of Diurnal Variation of Summer Rainfall over Subtropical East Asia

WEIHUA YUAN

LASG, Institute of Atmospheric Physics, Chinese Academy of Sciences, and Graduate School of the Chinese Academy of Sciences, Beijing, China

RUCONG YU

LASW, Chinese Academy of Meteorological Sciences, China Meteorological Administration, Beijing, China

MINGHUA ZHANG

Institute for Terrestrial and Planetary Atmospheres, School of Marine and Atmospheric Sciences, Stony Brook University, Stony Brook, New York

WUYIN LIN

Brookhaven National Laboratory, Brookhaven, New York

HAOMING CHEN AND JIAN LI

Chinese Academy of Meteorological Sciences, China Meteorological Administration, Beijing, China

(Manuscript received 22 May 2011, in final form 1 November 2011)

ABSTRACT

Using hourly rain gauge records and Tropical Rainfall Measuring Mission 3B42 from 1998 to 2006, the authors present an analysis of the diurnal characteristics of summer rainfall over subtropical East Asia. The study shows that there are four different regimes of distinct diurnal variation of rainfall in both the rain gauge and the satellite data. They are located over the Tibetan Plateau with late-afternoon and midnight peaks, in the western China plain with midnight to early-morning peaks, in the eastern China plain with double peaks in late afternoon and early morning, and over the East China Sea with an early-morning peak. No propagation of diurnal phases is found from the land to the ocean across the coastlines. The different diurnal regimes are highly correlated with the inhomogeneous underlying surface, such as the plateau, plain, and ocean, with physical mechanisms consistent with the large-scale "mountain–valley" and "land–sea" breezes and convective instability. These diurnal characteristics over subtropical East Asia can be used as diagnostic metrics to evaluate the physical parameterization and hydrological cycle of climate models over East Asia.

1. Introduction

Previous studies have shown that the complex topographic effect can result in distinctive—even unique—climate features over subtropical East Asia, such as the largest midlevel cloud cover of continental stratus in early spring (Yu et al. 2004) and the distinct mei-yu frontal zone during summer monsoon season (Ding 1992). Diurnal variability of rainfall is also an important aspect of regional climate (Yang and Slingo 2001) and has been extensively studied for several decades. The inhomogeneous surface types over subtropical East Asia, such as plateau, plain, basin, and sea (Fig. 1), cause robust regional-scale diurnal features of summer rainfall. Understanding these features and the underlying physical mechanisms is not only important to predicting regional precipitation events but also valuable as a powerful tool to identifying and correcting model deficiencies (Lin et al. 2000; Trenberth et al. 2003).

Studies on precipitation diurnal variation over subtropical East Asia can be traced back to several decades ago. Early literature employing limited rain gauge data

Corresponding author address: Rucong Yu, LASW, Chinese Academy of Meteorological Sciences, China Meteorological Administration, No. 46, Zhongguancun Nandajie, Beijing 100081, China. E-mail: yrc@lasg.iap.ac.cn
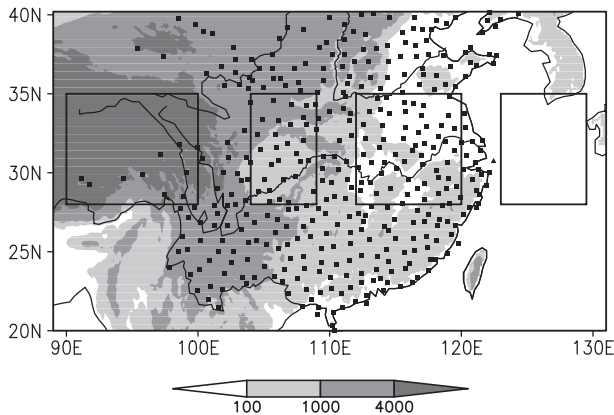
FIG. 1. Surface elevation (shaded, m) over subtropical East Asia, together with locations of the 394 rain gauge stations (black squares and one triangle) used in this study. The triangle represents the Chongming Island station. The four subregions are outlined for regional average.

reported dominant nocturnal rainfall over the Tibetan Plateau (Ye and Gao 1979) and the Sichuan basin (Lu 1942). Ramage (1952) found significant afternoon peak at stations of inland China but early-morning maximum on several islands along the coastline of China, Japan, and Korea. In addition, other studies have also reported about rainfall diurnal variations of China based on data of limited regions or periods (Wang et al. 2004; Fujinami et al. 2005; Zhao et al. 2005).

Using records from 706 rain gauges, Yu et al. (2007b) carried out a comprehensive analysis of rainfall variability over the contiguous China and pointed out that summer precipitation has distinct diurnal variations with considerable regional features. Over the southern inland and northeastern China, summer rainfall peaks in late afternoon. The late-afternoon rainfall peak over the land areas can be explained by the diurnal variation of low-level atmospheric instability caused by solar heating. Meanwhile, the afternoon prevailing sea breeze, against the mountains in southern China, results in low-level convergence and more water vapor, which also contributes to the late-afternoon rainfall maximum in that area (Yu et al. 2009). Rainfall in southwestern China presents primary midnight and early-morning diurnal peaks, which were also recognized in other studies using both station records (Lu 1942; Johnson et al. 1993; Peng et al. 1994; Yin et al. 2009; Wang et al. 2011) and satellite observations (Zhou et al. 2008; Chen et al. 2009; Xu and Zipser 2011). In central eastern China, the rain gauge data indicate that there are no uniform diurnal peaks across different stations (Yu et al. 2007b; He and Zhang 2010), and that the regionally averaged rainfall has two comparable diurnal peaks; one in the late afternoon and the other in the early morning (Yu et al. 2007b). The physical

mechanisms behind the prevailing nocturnal rainfall peak have not been clearly understood up to now. The nocturnal rainfall over southwestern China is shown to be partly related to the radiative cooling at the cloud top during night (Lin et al. 2000) and to the diurnal clockwise rotation of the lower-tropospheric circulation, especially the accelerated nocturnal southwesterlies (Chen et al. 2010). The early-morning rainfall peaks over eastern China are found to mainly exist in the active summer monsoon period, whereas the late-afternoon rainfall peaks dominate in the break period (Yuan et al. 2010).

There are few comprehensive studies on the rainfall diurnal variation over the oceans around China. Studies are usually confined to areas such as the South China Sea (Ohsawa et al. 2001; Lu and Xu 2007; Aves and Johnson 2008; Li et al. 2010) or to the several islands of China and Japan (Ramage 1952). Most of the studies reported a dominant early-morning diurnal peak in the oceanic areas and a propagating signal from the southern coastline of mainland China to the northern South China Sea southeastwardly. The rainfall diurnal features over the East China Sea have not been investigated in the past.

As studies based on in situ (rain gauge, radar) datasets were always restricted by some type of spatial or temporal sampling limitation, more and more studies of the diurnal variability of rainfall prefer to using satellite data. Numerous studies have proved that satellite observations present comparable diurnal features with the station rain gauges over global or regional areas and provide a great opportunity to comprehensively understand the diurnal precipitation processes, especially over the oceans (e.g., Yang and Slingo 2001; Yang and Smith 2006; Huffman et al. 2007; Dai et al. 2007). Based on the intercomparison of the rainfall diurnal features between the rain gauge and satellite data, the objective of this study is to show four distinct regimes of diurnal features of summer rainfall over subtropical East Asia, including the features over the subtropical seas and the Tibetan Plateau, which have not been fully understood before. Specifically, we identified four different regimes of diurnal rainfall variation with different underlying surface types or elevations and diurnal features, which are represented by the four boxes in Fig. 1. These are the Tibetan Plateau (TP), defined to be the most elevated region (28°–35°N, 90°–100°E) with a mean elevation of 4452 m; the western plain (28°–35°N, 103°–109°E) and the eastern plain (28°–35°N, 112°–120°E) with mean elevations of 1203 and 135 m, respectively, and distinct diurnal variations; and the East China Sea (28°–35°N, 122°–130°E). The simulations of the diurnal cycles of the hydrological processes in East Asia are still big challenges for global and regional climate models (Betts and Jakob 2002; Dai and Trenberth 2004; Huang et al. 2008; Wang and Zhang 2009). The characterization of the

diurnal rainfall over subtropical East Asia can be used as metrics in evaluating climate models.

The rest of the paper is organized as follows. Section 2 describes the datasets. Section 3 shows the summer mean rainfall and low-level circulations. Section 4 shows the spatial distributions of diurnal peaks over subtropical East Asia and a comparison of rain gauge and satellite data. Section 5 highlights the analysis of regional features. Section 6 presents the diurnal characteristics of summer rainfall as a function of longitudes. Section 7 discusses the possible physical mechanisms behind the diurnal features over the four regimes. The summary and concluding remarks are given in section 8.

2. Data

Hourly rain gauge data (Gdata) from 394 stations are used in this study, which were collected and compiled by the National Meteorological Information Centre (NMIC) of the China Meteorological Administration (Yuan et al. 2010). The records of rain gauge data were made by siphon or tipping-bucket rain gauges and were collected automatically by computer. The dataset has been quality controlled by NMIC, which consists of a climatological limit value test, a station extreme value test, and an internal consistency test. Additionally, these hourly data have been compared with daily rainfall data, which are observed by rain gauge glass, and records that have large discrepancy between the two datasets have been regarded as missing values. Detailed information can be found in Li et al. (2011). Of the 394 stations, 83% have more than 700 days of records without missing values. The locations of the stations are shown in Fig. 1.

The Tropical Rainfall Measuring Mission (TRMM) 3B42 (3 hourly, 0.25°) precipitation data are also used in this study (Huffman et al. 2007). This dataset was created by blending passive microwave data collected by the TRMM Microwave Image (TMI), the Special Sensor Microwave Imager, the Advanced Microwave Scanning Radiometer for Earth Observing System, the Advanced Microwave Sounding Unit B, and the infrared (IR) data collected by the international constellation of geosynchronous earth-orbit satellites based on calibration by the precipitation estimate of the TMI and precipitation radar (PR) combined algorithm. When there are multiple overpasses in the 3-hourly window for a given grid box, the average is used. A simple approach has been adopted to combine the microwave and IR estimates: the physically based combined microwave estimates (mean values when multiple overpasses exist in the 3-hourly window) are taken "as is" where available and the remaining grid boxes are filled with microwave-calibrated IR estimates. The current "full" microwave measurement covers about 80% of the earth's surface in the latitude band 50°N–S, and a gauge correction was applied over land (Huffman et al. 2007).

TRMM PR data (product 2A25) are also used. The rainfall in 2A25 is classified into three types: convective, stratiform, and "other" (Iguchi et al. 2000). Simply, a stratiform profile is classified if the PR detects a bright band near the freezing level in the profile. If no bright band exists and if any value of radar reflectivity in the beam exceeds 39 dBZ, then the profile is labeled convective. Exceptions to both convective and stratiform are labeled as "other" in the dataset. Over subtropical East Asia, the convective and stratiform rainfall total more than 90% of the total rainfall amount.

Previous studies have pointed out discrepancies of diurnal rainfall between rain gauge and TRMM satellite data in different regions of the world (Wang et al. 2004; Liu et al. 2009; Dai et al. 2007; Huffman et al. 2007; Sapiano and Arkin 2009; Kikuchi and Wang 2008). Sorooshian et al. (2002) used Precipitation Estimation from Remotely Sensed Information using Artificial Neural Networks (PERSIANN) and showed that PERSIANN tends to underestimate rainfall late at night and in the morning and tends to overestimate rainfall during the afternoon and evening, when they compare diurnal cycles derived from PERSIANN and from in situ radar over Brazil.

The ways that satellite and station rain gauges measure the precipitation are totally different. Techniques for evaluating precipitation from satellites may be divided into those based on visible or IR measurements, those based on passive microwave measurements, and those based on radar measurements (Kidder and Vonder Haar 1995; Masunaga et al. 2002). Satellite algorithms using visible and IR techniques provide excellent temporal and spatial sampling from geostationary orbits, but this technique relies on the assumption that correspondences exist between cloud radiances and rain rates. Estimates are subject to threshold biases and contamination by nonraining cirrus (Todd et al. 1999). The microwave radiometer affords a more direct inference of precipitation. It observes the integrated effects of radiation both emitted from the surface and hydrometeors and scattered by solid hydrometeors. The main source of attenuation of microwave radiation is scattering due to ice or liquid hydrometeors. The microwave measurements are affected by surface emissivity and sampling biases. The rain gauge observation is mostly reliable, which directly measures surface precipitation. But it has the major disadvantage of measuring only what is falling within an area tens of centimeters in diameter. Inferences about what might have fallen in tens of square kilometers around the gauge can only be made to the extent that what the gauge encounters is representative of what happened in the surrounding

area, especially over the regions with complex terrain. Moreover, gauges in mountain areas are usually situated in valleys for convenient maintenance and therefore may not represent the true areal-averaged rainfall that a satellite sees.

In view of these limitations, we have used both rain gauge and satellite data. We examine the consistent diurnal features in the two datasets, and when they are different, we discuss which one is more reliable.

The Japanese 25-yr Reanalysis (JRA-25; Onogi et al. 2007) is employed to describe the large-scale circulations. In this paper, we also used the contrast between moist static energy temperature (T_{MSE}) and saturated moist static energy temperature (T_{MSE}^*) computed from JRA-25 as a measure for the likelihood of moist convection. The T_{MSE} is defined as

$$T_{MSE} = (gz + Lq)/c_p + T,$$

where T is temperature, q is the specific humidity, z is height, c_p is the specific heat of air, L is the latent heat of evaporation, and g is gravitational acceleration; T_{MSE}^* is defined similarly, with q being replaced by the saturated specific humidity.

All the datasets used are from 1998 to 2006, June–August. The measurable precipitation is defined here as ≥ 0.1 mm h^{-1} for both rain gauge and satellite observations. Following Zhou et al. (2008), the hourly mean rainfall frequency (intensity) is defined as the percentage of observational hours having measurable precipitation (the mean rate in precipitation hours). Four periods [based on local solar time (LST)] are defined: midnight (from 2000 to 0200 LST), early morning (from 0200 to 0800 LST), noon (from 0800 to 1400 LST), and late afternoon (from 1400 to 2000 LST).

3. Summer mean rainfall and low-level circulations

Before analyzing the diurnal cycle of precipitation, the summer mean rainfall amount and 850-hPa winds in TRMM 3B42 and JRA-25 are shown at first in Fig. 2. The 3B42 has the proven ability to capture rainfall distributions on monthly or longer time scale, especially over land areas (Huffman et al. 2007; Zhou et al. 2008).

Based on 3B42, summer rainfall over subtropical East Asia mainly presents two rain belts. One, known as the subtropical mei-yu/bai-u front, exhibits a zonally elongated structure extending from east China toward the northwestern Pacific near 30°N, with heavy rainfall along the Yangtze River (100°–120°E) in China, and extending over South Korea. The other locates along the southern slope of the Himalayas to the South China Sea (around 20°N), reflecting the influences of monsoon and tropical rainfall systems, as well as the topographic effect.

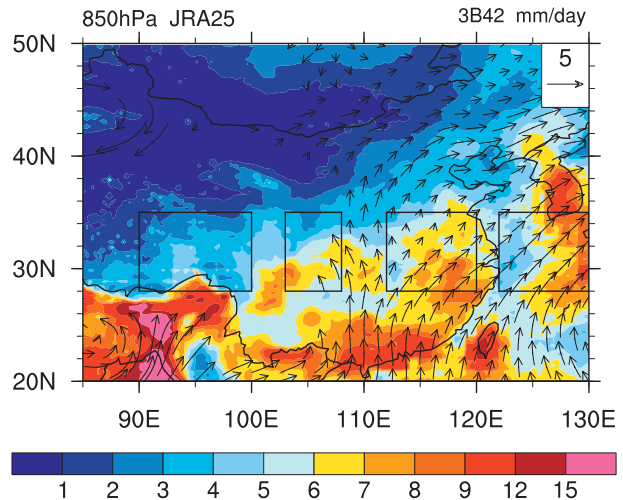FIG. 2. Summer (June–August) mean precipitation (unit: mm day^{-1}) and 850-hPa wind fields (unit: m s^{-1}) in TRMM 3B42 and JRA-25.

The rainfall distribution is closely related to large-scale circulation. In the lower troposphere (850 hPa), southwesterly flow prevails over southeastern China (Fig. 2). A cyclonic circulation exists in the Upper Yangtze River valley with significantly reduced wind speed around 30°N. The combination of the southwest vortex and the low-level convergence of the warm tropical water vapor provide a favorable environment to maintain the rainfall systems along the Yangtze River (Tao and Chen 1987; Zhou and Yu 2005).

4. Spatial distributions of diurnal peaks over subtropical East Asia

Figure 3 compares the diurnal peaks derived from station data and TRMM 3B42. Orange and red mean the noon to late-afternoon peaks; blue and green mean the midnight and early-morning peaks. Summer rainfall over subtropical East Asia manifests pronounced diurnal variations with considerable regional features.

The rain gauge data shows a uniform nocturnal peak in rainfall amount at stations over the Tibetan Plateau (Fig. 3a), which has also been found in previous studies (Yu et al. 2007b; Yin et al. 2009). However, the satellite product shows late-afternoon to early-evening rainfall diurnal peaks over most of the plateau; the rainfall maximum around midnight or early morning only exists in the southeastern periphery of the plateau (Fig. 3b). It has been pointed out that the afternoon (morning) rainfall in satellite data tends to be overestimated (underestimated) over many land areas (Dai et al. 2007; Sapiano and Arkin 2009). The overestimation/underestimation may be related to the sensitivity/insensitivity of microwave estimates to the particles with/without ice content and different cloud
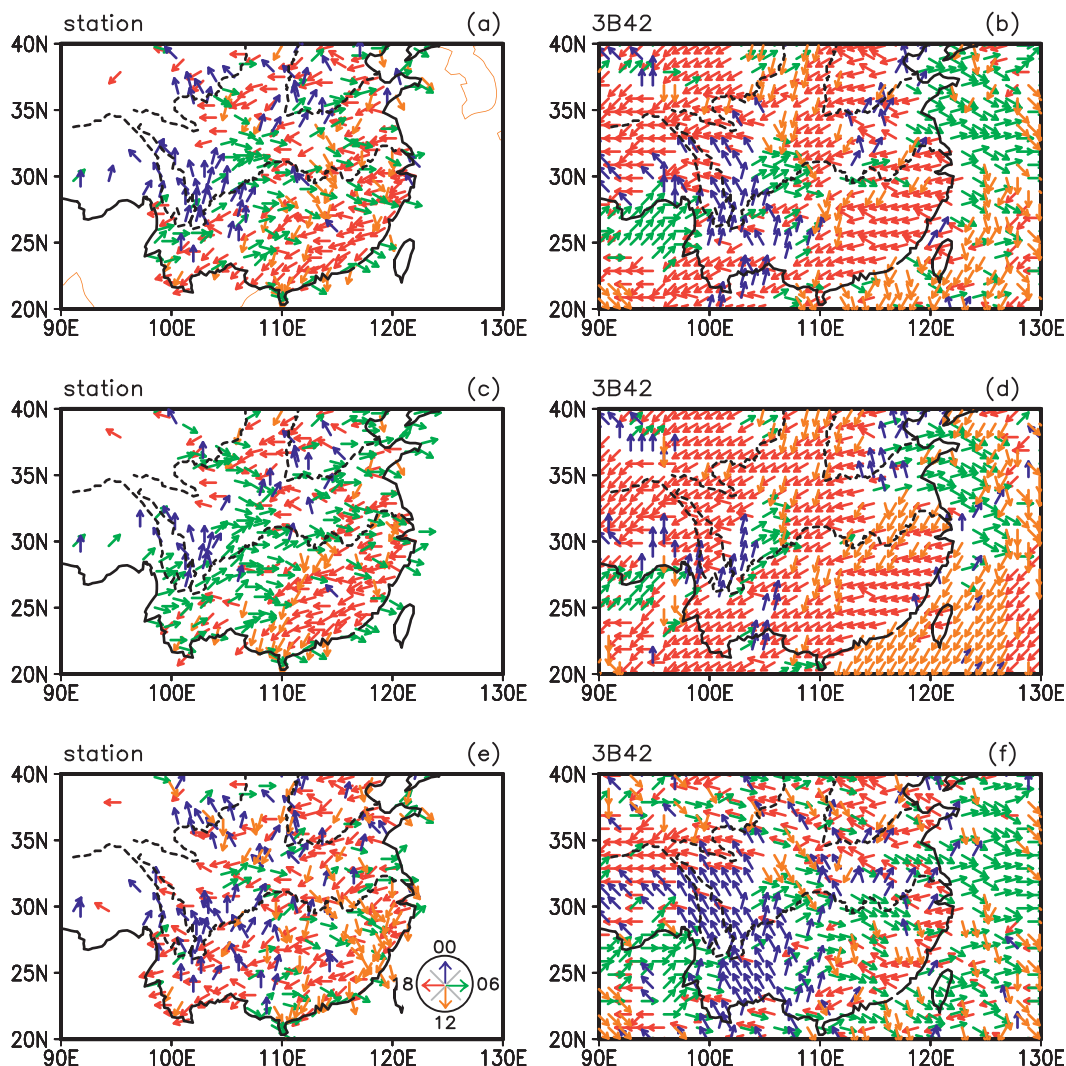
FIG. 3. Spatial distributions of the diurnal peaks of summer rainfall (top) amount, (middle) frequency, and (bottom) intensity derived from (left) station rain gauge data and (right) TRMM 3B42. The unit vectors denote the LST of the hourly maximum precipitation. The green (blue) vectors represent the diurnal peaks occurring between 0200 and 0800 (2000 and 0200) LST, and the red (orange) vectors for those peaks occurring between 1400 and 2000 (0800 and 1400) LST. The Yangtze and Yellow Rivers are drawn as black dashed lines.

features in these two periods. Especially over the plateau, which may still be covered by snow even in summer, the influence of ice scattering may be greater than anywhere else. But based on the following two evidences, we still argue that the late-afternoon peak should exist in the area-averaged rainfall diurnal variation over the TP. First, a recent study by Chen et al. (2012) showed that rain gauge stations on mountain ridges over the TP from a field experiment displayed an afternoon diurnal peak instead of a nocturnal peak as routine stations in valleys. The 10 meteorological stations over the TP in the present study, locating in the leftmost box in Fig. 1, are sited mostly in valleys for easy access and maintenance. The average elevation of the 10 stations is about 3104 m;

however, the elevation of the surroundings, which is defined as the grids with the distance to the stations having less than 1°, is about 4218 m. Second, Singh and Nakamura (2009), using a very high-resolution (5 km × 5 km) TRMM 2A25 product for a portion of the TP, found nocturnal diurnal peaks over the TP valleys and late-afternoon diurnal peaks over the ridges. This is consistent with the analysis by Chen et al. (2012), who use field experimental data for a smaller domain. The nocturnal rainfall diurnal peak revealed by the routine station data should mainly occur in the TP valleys. Based on these results, we will cautiously characterize the regional averaged diurnal peaks over the plateau as occurring both in the late-afternoon and midnight periods. The late-afternoon rainfall

peak would mainly occur on the mountains over the TP, while the midnight one in the valleys over the TP. This relationship of rainfall peak time with surface terrain over the TP will be also shown later in our analysis.

In southwestern China, the land areas adjacent to the plateau, significant midnight to early-morning diurnal peaks of rainfall amount are found, and this feature is largely consistent between the two datasets (Figs. 3a,b).

In eastern China, the land areas east of 110°E, the late-afternoon rainfall peaks dominate in both datasets. Early-morning and midnight diurnal peaks can also been found at some locations in this region (Figs. 3a,b). The areas where the rainfall amount has early-morning diurnal peaks are relatively smaller in 3B42 (Fig. 3b) than those in Gdata (Fig. 3a). Eastern China has much smooth terrain, and the density of the stations is much higher than that of the TP. The topographic effect to the Gdata should be small. Moreover, there have already been some explanations of the early-morning rainfall diurnal peak over this area, which is mostly contributed by the rainfall with longer duration time (Yu et al. 2007a) and is closely related to the large-scale forcing (Chen 1983; Chen et al. 2010; Yuan et al. 2010). Similar differences between rain gauge and satellite measurements have also been found in other regions of the world. As pointed out by previous studies employing data from satellites carrying IR or microwave radiometers, satellite products tend to exhibit more afternoon and early-evening rainfall than that in surface observations averaged over the United States and tropical land areas (Dai et al. 2007; Huffman et al. 2007; Sapiano and Arkin 2009; Kikuchi and Wang, 2008). Therefore, we believe that the rainfall over eastern China is dominated by a late-afternoon peak with a secondary early-morning peak.

Over the East China Sea, the rainfall amount in the satellite data is at the hourly maximum around the early morning (Fig. 3b). The rainfall at some stations along the coastlines also manifests the early-morning diurnal peaks (Fig. 3a).

The diurnal variation of precipitation can be from either that of precipitation frequency or intensity. The peak time of frequency (Figs. 3c,d) is found to be generally consistent with that of rainfall amount. The rainfall intensity (Figs. 3e,f) shows less coherent phases in both rainfall products. For Gdata, diurnal peaks of the frequency occurring in the early morning increase (Fig. 3c) when compared with the amount (Fig. 3a), while the intensity has more midnight and noon phases (Fig. 3e) than rainfall amount (Fig. 3a). The late-afternoon peaks of rainfall frequency tend to be overestimated in 3B42 (Fig. 3d) relative to Gdata (Fig. 3c). About 60% of the stations have midnight and early-morning diurnal peaks of frequency in the regions between 28°–35°N and 100°–120°E,

compared to only 22% of the grids in 3B42. In contrast to the frequency, the intensity of 3B42 exhibits more midnight to early-morning maximum (about 67%, Fig. 3f) than that of Gdata (about 44%, Fig. 3e). According to Zhou et al. (2008), TRMM 3B42 shows larger late-afternoon frequency and stronger early-morning intensity in central eastern China compared with Gdata. The discrepancy over central eastern China could be attributed to the overestimated late-afternoon rainfall and the underestimated early-morning light rainfall in 3B42 (Yuan et al. 2012). It is likely that the overestimation or underestimation may also exist in the western plain. Sanderson et al. (2006) pointed out that the morning rainfall has less ice content. The underestimation of morning rainfall might be due to the lack of sensitivity of microwave radiation to particles without ice at the frequencies used for rainfall monitoring. But further studies are required.

5. Regional diurnal features

a. Diurnal features in the three regimes over the land in the rain gauge and satellite measurements

To further illustrate the diurnal features of rainfall, we use Fig. 4 to show the hourly rainfall amount, frequency, and intensity from Gdata (solid lines) and 3B42 (dotted lines) averaged in the TP, and western and eastern plains.

Over the TP (top row in Fig. 4), the rainfall in Gdata presents uniform nocturnal diurnal phases in amount, frequency, and intensity. The intensity peaks earlier at 2100 LST (Fig. 4c), while the frequency is at a maximum at 0200 LST (Fig. 4b) and the amount peaks at 0000 LST (Fig. 4a). For 3B42, the diurnal peaks of the rainfall amount, frequency, and intensity also show similar diurnal phases but in the late afternoon. The frequency (Fig. 4b) peaks at 1500 LST, which is 3 h earlier than the amount and intensity (Figs. 4a,c).

In the western plain (middle row in Fig. 4), the rainfall amount of Gdata (Fig. 4d) manifests the significant nocturnal diurnal peak at about 0300 LST and the rainfall decreases sharply after sunrise with the minimum at 1400 LST. For 3B42 (Fig. 4d), the variation is similar to that of Gdata, with the correlation between the two lines exceeding 0.9. For the rainfall frequency (Fig. 4e), however, a large discrepancy exists between the two datasets, with the correlation being only 0.2. Gdata presents a significant early-morning diurnal peak, while 3B42 has its maximum around 1600 LST with weak amplitude. For the intensity (Fig. 4f), Gdata and 3B42 generally agree with each other, but the diurnal phase in the satellite product lags that of Gdata by a few hours.

In sharp contrast to the western domain, for the eastern plain (bottom row in Fig. 4), the rainfall amount (Fig. 4g) in both Gdata and 3B42 presents a dominate late-afternoon
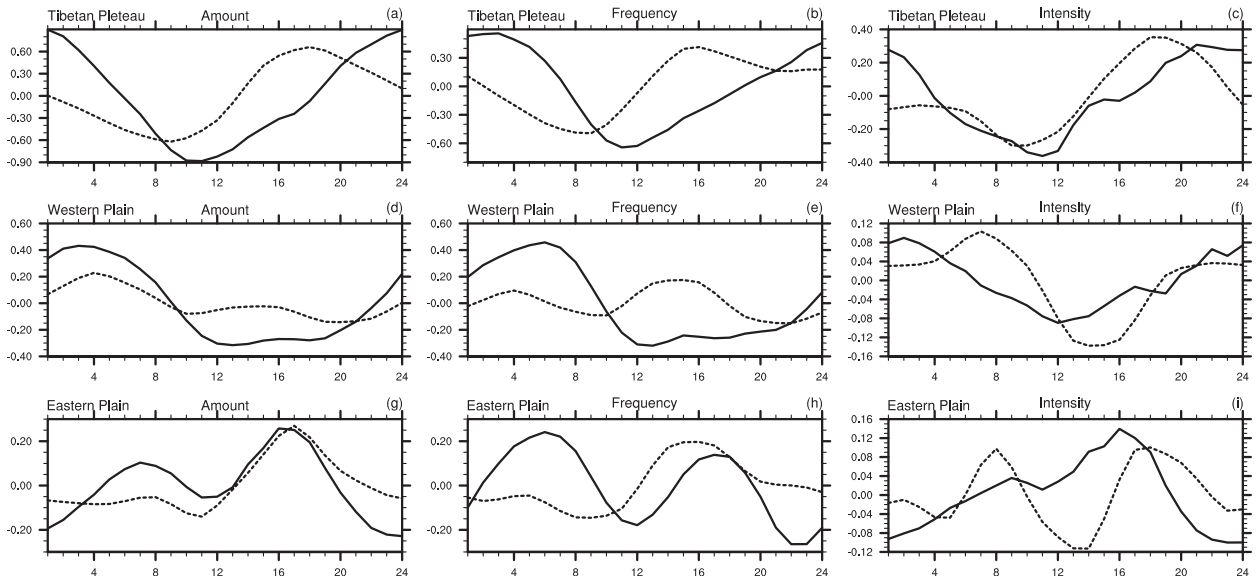
FIG. 4. The normalized (by the daily mean) diurnal cycles of summer precipitation (left) amount, (middle) frequency, and (right) intensity averaged in the (top) TP, (middle) western plain, and (bottom) eastern plain outlined in Fig. 1 from station rain gauge data (solid lines) and TRMM 3B42 (dotted lines).

diurnal peak. There is a secondary hourly maximum in the early morning, which is more pronounced in Gdata than in 3B42. The frequency (Fig. 4h) in gauge data shows two comparable peaks, with one in the early morning and the other later in the afternoon. The satellite product only captures the late-afternoon peak. For the rainfall intensity (Fig. 4i), both datasets exhibit double peaks in the early morning and late afternoon. But different from the frequency, the early-morning rainfall intensity in 3B42 is stronger than that in Gdata. Similar to the western plain, the correlation coefficient between the two datasets of rainfall amount is higher than that of both the frequency and intensity.

b. The rainfall diurnal features over the East China Sea

In addition to the peak hour shown in Fig. 3, we analyzed the regionally averaged diurnal features of the rainfall amount, frequency, and intensity (Fig. 5) and the diurnal characteristics along the coastlines (Fig. 6) over the East China Sea in this section.

As shown in Fig. 5, the rainfall amount in TRMM 3B42 reaches the maximum at about 0600 LST and the minimum at 2300 LST. Except for the early-morning peak, the rainfall frequency over the East China Sea is also elevated in the evening. The variation of intensity is relatively small and persists at a high level from midnight to early afternoon. To validate the results in 3B42, we also calculate the rainfall diurnal features at Chongming Island (marked by a triangle in Fig. 1). The rainfall

amount and frequency have the hourly maximum in the early morning, similar to those in 3B42. The frequency peaks at 0500 LST, which is 2 h earlier than the rainfall amount in Gdata. The intensity increases from the early morning with the peak occurring around 1500 LST and a secondary diurnal peak occurring at 2300 LST. For the rainfall amount, frequency, and intensity, the diurnal variations between 3B42 and Gdata are fairly consistent, giving us the confidence in the diurnal features derived from 3B42 over the East China Sea.

Figure 6 illustrates the mean diurnal variations of the average rainfall amount between 28° and 35°N from TRMM 3B42 and 2A25, as a function of the distance away from the coastlines. The x axis represents the distances to the coastlines (marked by the dashed lines). The negative values denote the landmass, and the positive values denote the oceanic areas. The most distinctive feature in the total rainfall (Fig. 6a) is the dominant late-afternoon peak over land, but there is a significant early-morning peak over the seas. It is noted that the diurnal phases across the coastline do not exhibit propagating characteristics, which is different from the tropical oceans (Yang and Slingo 2001; Ichikawa and Yasunari 2006; Aves and Johnson 2008). To identify what kind of rainfall (convective or stratiform rainfall) mainly contributes to the different diurnal features over the land and sea areas, the mean diurnal variations of convective and stratiform rainfall amount derived from TRMM 2A25 are calculated. As indicated in Fig. 6b, the convective rainfall shows pronounced late-afternoon peak in the land and
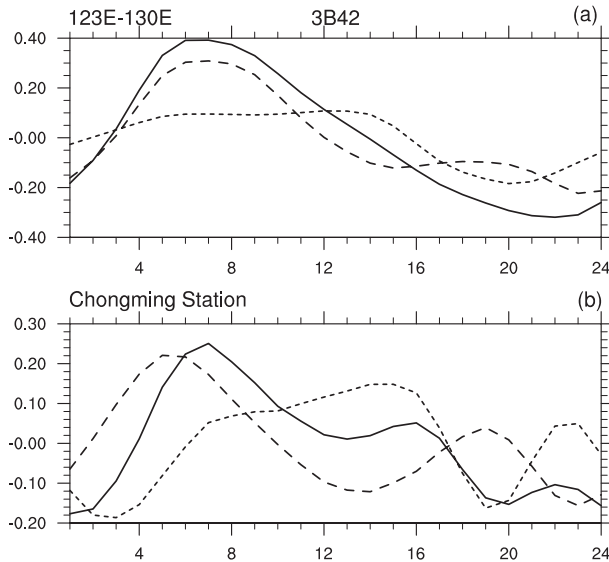
FIG. 5. The normalized (by the daily mean) diurnal cycles of summer precipitation amount (solid line), frequency (dashed line), and intensity (dotted line) averaged (a) over the East China Sea outlined in Fig. 1 from TRMM 3B42 and (b) at Chongming Island station marked by a triangle in Fig. 1 from the station rain gauge data.

the diurnal phase shifts to early morning around the coastlines, while the peak hour of stratiform rainfall does not vary from the land to the sea (Fig. 6c). The distinct diurnal features between different underlying surfaces are greatly contributed by the convective rainfall.

6. The longitudinal diurnal characteristic of summer rainfall

On the basis of the significant regional diurnal features presented above, the longitudinal diurnal characteristic of rainfall amount, taking subtropical East Asia as a whole, is illustrated in Fig. 7.

From the TP to the East China Sea, the rainfall amount averaged between 28° and 35°N shows the eastward-delayed diurnal phases in both 3B42 (Fig. 7a) and Gdata (Fig. 7b). The delayed features are most obvious over the western plain, extending for about 1000 km, while the diurnal peak shifts to about 1600 LST around 110°E in 3B42, different from 0800 LST in Gdata. According to Chen et al. (2010), this delayed feature is thought to be due to the diurnal clockwise rotation of the lower-tropospheric circulation and is mostly contributed by the rainfall events lasting longer than 6 h. As the long-duration rainfall experiences coincident movement with the summer monsoon circulations (Yuan et al. 2010), the delayed features would also experience variations in the subseasonal time scale (Xu and Zipser 2011). Over the whole TP, the rainfall in both datasets presents uniform phases, while the peak time in Gdata lags that in 3B42 by about 4 h.

The secondary peak in the early morning over the eastern plain is absent in 3B42. A sharp contrast in the diurnal phases between the land and sea areas is obvious in both datasets, and no propagating features are found (Fig. 7a).

In Gdata, the rainfall frequency (Fig. 7d) shows a similar phase-delayed feature as that in the rainfall amount (Fig. 7b), but with a much stronger early-morning rainfall peak over the eastern plain. Although the feature of rainfall amount in 3B42 is generally similar to that in Gdata, the phase-delayed feature is almost obscured in the frequency (Fig. 7c), as the midnight and early-morning rainfall frequencies in the western plain are underestimated in 3B42 (Figs. 3, 4). The late-afternoon diurnal rainfall maximum persists from the TP to the coastline (Fig. 7c). If employing 3B42 for diurnal analyses over East Asia, more cautions should be given when using the features in frequency and intensity. As the rainfall intensity exhibits less coherent diurnal phases in both Gdata and 3B42, the full diurnal characteristic is weaker than that of rainfall amount and frequency (figure not shown).

So, we summarize the full diurnal features of subtropical East Asia (Fig. 8) as follows: in the TP, rainfall occurs in the late afternoon (as shown in 3B42) and at midnight (as shown in Gdata); from the TP to the western plain, the diurnal peak delays from midnight to early morning; when moving to the eastern plain, late-afternoon rainfall, which is mainly contributed by the rainfall intensity, dominates the total rainfall, with a secondary peak in the early morning mainly from rainfall frequency; over the East China Sea, rainfall mainly occurs in the early morning.

The diurnal phase is found to be highly correlated with the complex topography over subtropical East Asia with its combined distributions of plateau, plain, and sea. Figure 9 illustrates the longitudinal variations of percentages of the late-afternoon (solid lines) and early-morning (dashed lines) rainfall to total rainfall amount as well as the surface elevations averaged between 28° and 35°N. Over the TP, the late-afternoon rainfall dominates the total rainfall amount in 3B42 (Fig. 9a). Eastward along with the variations of the elevation, the rainfall occurring in the late afternoon experiences variations consistent with the topography, with high elevation corresponding to a larger percentage of late-afternoon rainfall and vice versa. Especially notable is that around the Yarlung Zangbo Grand Canyon (about 95°E), where the late-afternoon rainfall amount in 3B42 declines to be almost equal to the early-morning one. Although the early-morning rainfall dominates the total rainfall in Gdata (Fig. 9b), the impact of topography on the occurrence of rainfall is still obvious. The late-afternoon rainfall shows a similar variation to that of topography and reaches an extremely low level around the canyon. In the adjacent plains, the percentages of late-afternoon rainfall fall
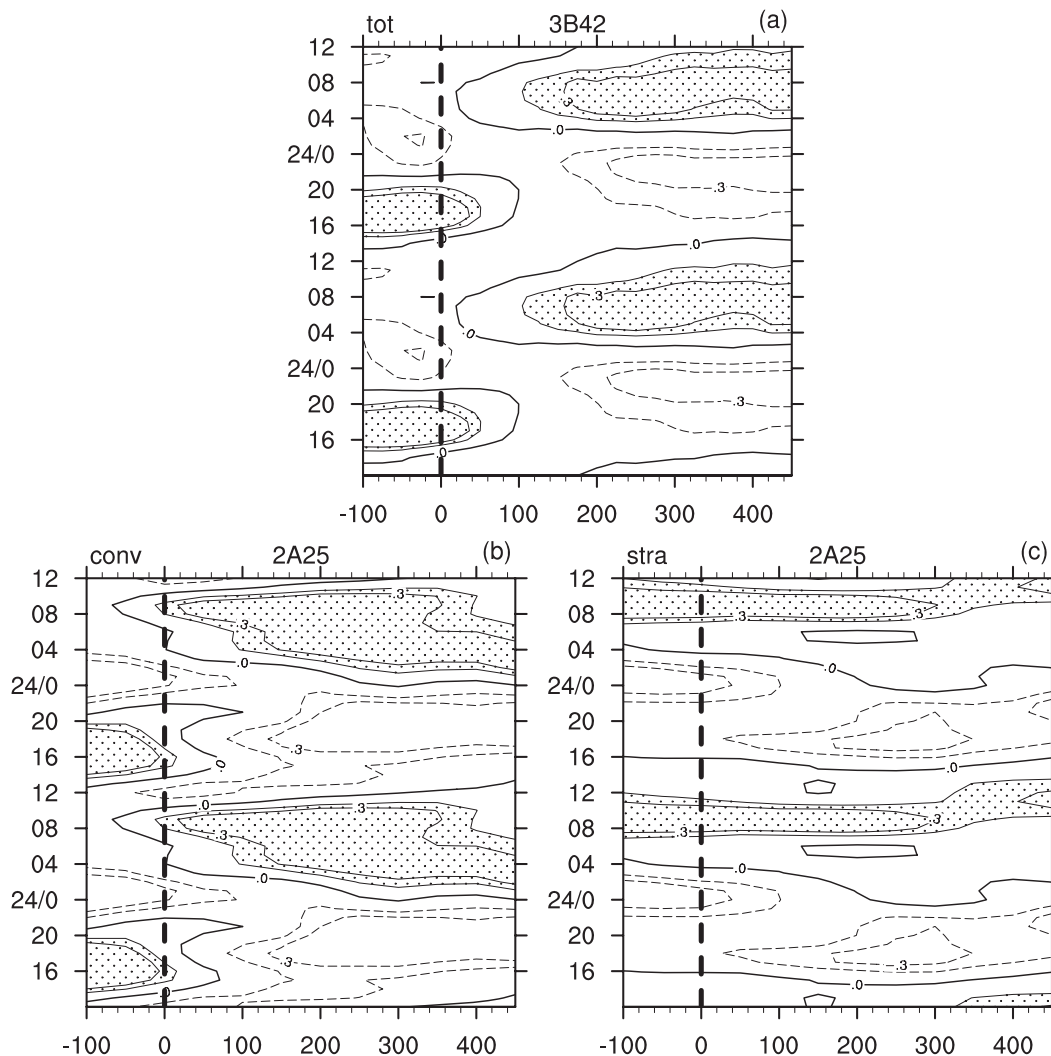
FIG. 6. Diurnal variations of rainfall amount (normalized by the daily mean) (a) averaged between 28° and 35°N of TRMM 3B42 as a function of the distance from the coastlines. (b),(c) As in (a), but for the (b) convective and (c) stratiform rainfall amount from TRMM 2A25. The black vertical dashed lines represent the coastlines. The x axis represents the distances to the coastlines. The negative values (km) denote the landmass and the positive ones for the sea areas.

sharply along with the decline of the elevation, while the early-morning rainfall becomes large, and it is fairly consistent between the two datasets. Over the east edge of the western plain, the proportion of late-afternoon rainfall gradually increases along with the elevated terrain, maintaining a stable value over the eastern plain and reaching maximum near the coastline (Figs. 9a,b). Around the coastlines, the percentages of late-afternoon rainfall decrease and the early-morning rainfall dominate over the East China Sea (Figs. 9a,b).

7. Discussion

The influence of the large-scale "mountain–valley winds" on the rainfall diurnal cycle was first mentioned by Bleeker and Andre (1951), who focused on the diurnal features of the United States. For subtropical East Asia, the Tibetan Plateau, with a mean elevation of more than 4000 m above sea level, covers a region about a quarter of the size of the Chinese territory. At seasonal time scale, the Tibetan Plateau is a strong heat source in summer and sink in winter, functioning as an important modulator of the Asian climate (Yeh et al. 1957; Ye and Gao 1979; Yanai and Li 1994; Wu et al. 2007). The plateau is can be regarded as a "mountain" relative to the "valley," such as the western and eastern plains. At the diurnal time scale, the thermal effect of the Tibetan Plateau may also be a great factor to the diurnal feature over East Asia. The land–sea breeze often refers to vertical circulation along the coast that is directly forced
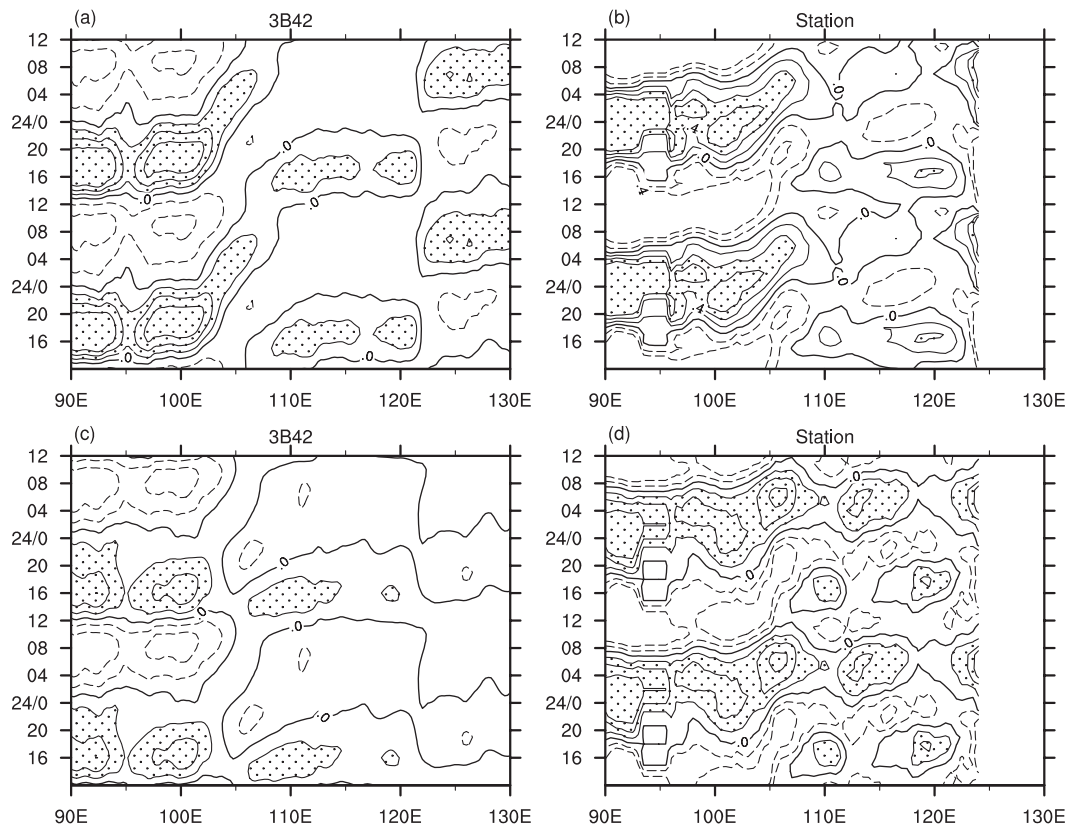
FIG. 7. Time–longitude distributions of the normalized (by the daily mean) diurnal variation of rainfall (top) amount and (bottom) frequency averaged between 28° and 35°N in (left) TRMM 3B42 and (right) rain gauge data.

by the thermal contrast between the land and sea, with spatial scales of less than a few hundred kilometers that are restricted to within the lower troposphere. This concept, however, has been generalized to also describe diurnal circulation patterns indirectly forced by large-scale thermal contrasts, such as the low-level jets. By analyzing the global surface wind and divergence fields, Dai and Deser (1999) pointed out that there exists a continental-scale land–ocean diurnal circulation, and that it is consistent with the diurnal variation of precipitation over the ocean and land areas. Over East Asia, Huang et al. (2010) also found that the local land–sea breeze circulation couples with the global-scale diurnal atmospheric pressure tide to produce a planetary-scale land–sea breeze with a spatial scale of 1000 km. The planetary-scale land–sea breeze mentioned in the Huang et al. (2010) paper covers the eastern plain. Their results also suggested the importance of low-level wind to the maximum diurnal rainfall over East Asia between summer and winter. The large-scale mountain–valley and "land–sea" effect may be one of the possible mechanisms of the diurnal variations of subtropical East Asia.

In afternoon to early evening, a warm diurnal temperature trough at 700–500 hPa can be found over the

TP (Fig. 11 in Chen et al. 2010). Corresponding to the thermal conditions, strong upward motions are found over the plateau. Averaged over the TP (black solid line in Fig. 10a), the maximum pressure vertical velocity exceeds 0.4 Pa s^{-1} near the surface of the plateau. Meanwhile, the maximum of T_{MSE} in the lower troposphere is quite close to the minimum of T_{MSE}^* at 1400 LST (Fig. 11a), which means that the thermal and moist condition is conducive to the occurrence of convection in the afternoon over the plateau.
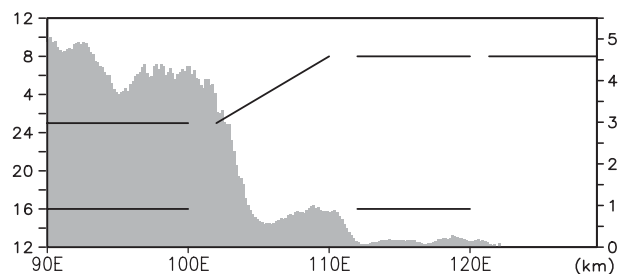

FIG. 8. Schematic diagram of the (left y axis) diurnal peak time (LST) over the four regimes summarized from station data and TRMM 3B42. The gray bars represent the (right y axis, km) elevations averaged between 28° and 35°N.
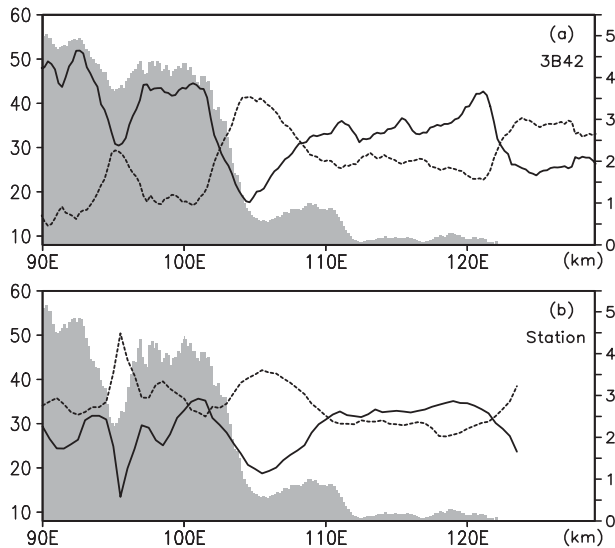
FIG. 9. Percentages (left, y axis) of late-afternoon (solid lines, 1400–2000 LST) and early-morning (dashed lines, 0200–0800 LST) rainfall to total rainfall amount in (a) TRMM 3B42 and (b) station data averaged between 28° and 35°N. The gray bars in (a) represent the (right y axis, km) elevations averaged between 28° and 35°N. The gray bars of 90°–100°E (100°–130°E) in (b) represent the (right y axis, km) elevations averaged between 28° and 30°N (28° and 35°N).

Influenced by the Tibetan Plateau, deep continental stratus cloud is found over the western plain, which hinders the solar radiation from reaching the ground (Yu et al. 2004; Li et al. 2005, 2008). The surface air temperature in the afternoon is relatively low over this area (Li et al. 2008). Combined with the eastward wind at the mid- and upper troposphere, an apparent warm and moist advection locates over the upper level of the western plain

(Fig. 11 in Chen et al. 2010). All these factors would suppress the development of static instability and the afternoon local thermal convection over the western plain.

During night, the zonal and vertical winds over the TP and western plain reverse (Figs. 7–10 in Chen et al. 2010). The plateau is controlled by subsiding airflow throughout the troposphere (black solid line in Fig. 10b). The anomalous airflow toward the TP (Figs. 7–10 in Chen et al. 2010) causes low-level convergence and upward motion over the plateau's eastern slope at night (gray dashed lines in Fig. 10b). Accompanied by the longwave radiative cooling at the cloud top (Lin et al. 2000) and the weak cold advection decreasing the stability (Chen et al. 2010), rainfall over the western plain is at a maximum precipitation during the midnight and early-morning periods.

The eastern plain can be regarded as the valley with respect to the TP, as well as the "land" relative to the East China Sea. Partly because of the influence of both the large-scale "sea breeze" in the afternoon and "mountain wind" at night, the percentages of late-afternoon and early-morning rainfall are fairly close to each other, compared to the other three regions (Fig. 9b). The proportion of late-afternoon rainfall that gradually increases from the eastern edge of the western plain to the coastlines could also be regarded as the competition between the large-scale mountain–valley and land–sea effects on the eastern plain. The complexity can also been found in the large-scale circulations. Additionally, acting as the land, positive convective available potential energy exists in the afternoon (Fig. 11b), and the vertical motion (black dashed lines in Fig. 10a) is upward at 1400 LST over the eastern plain. However, the pressure vertical velocity at 0200 LST in this area (black dashed lines in Fig. 10b) is also negative throughout the boundary layer to the
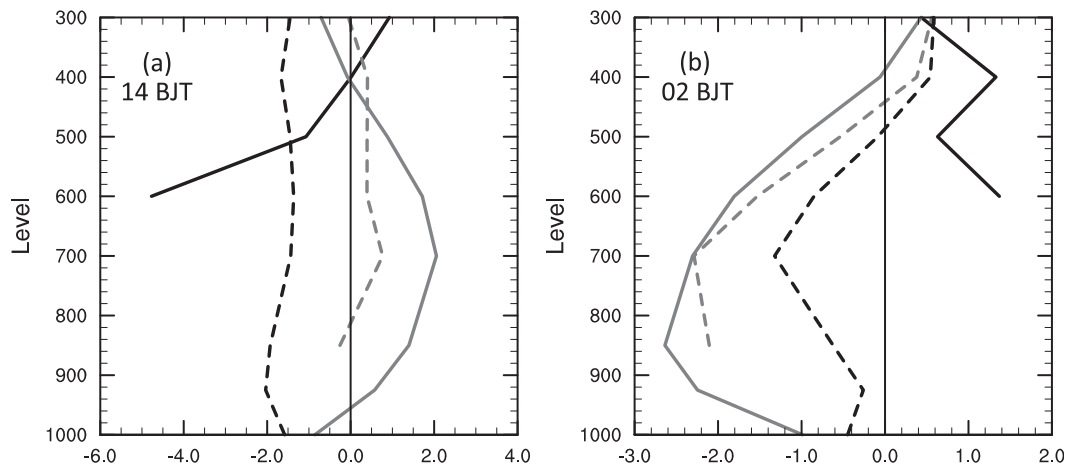

FIG. 10. Regional mean vertical profiles of omega (0.1 Pa s^{-1}) averaged in the TP (black solid lines), western plain (gray dashed lines), eastern plain (black dashed lines), and East China Sea (gray solid lines) at (a) 1400 and (b) 0200 Beijing time (BJT) from JRA-25.
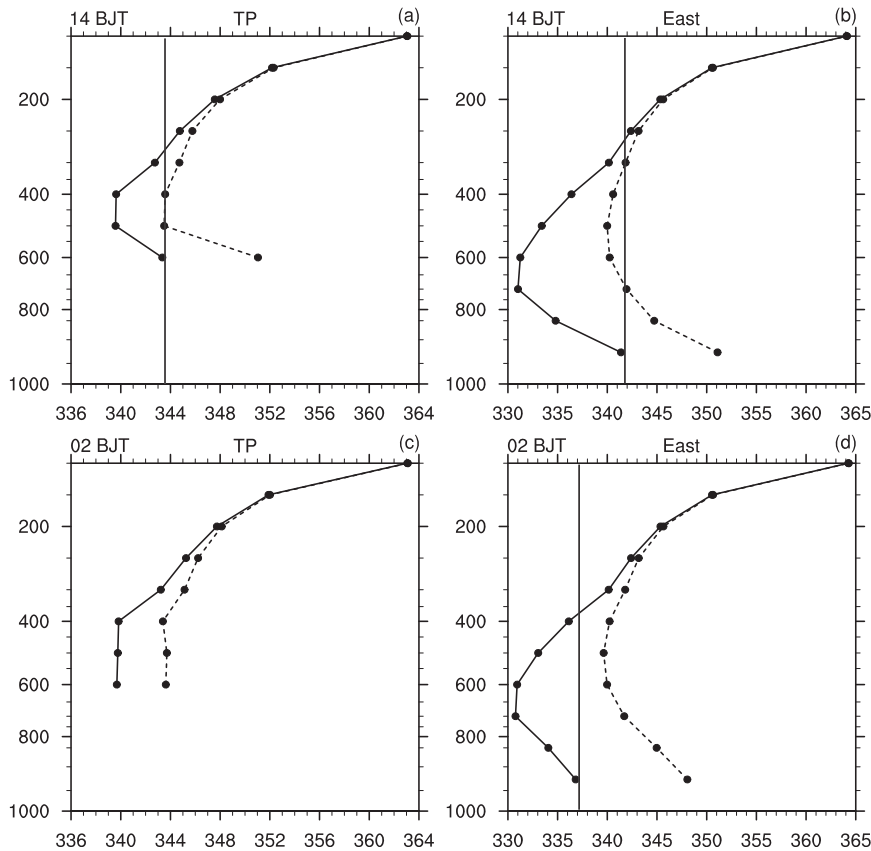
FIG. 11. Vertical distributions of the moist static energy (solid lines) and saturated moist static energy (dashed lines) temperature (K) averaged in the (left) TP and (right) eastern plain at (top) 1400 and (bottom) 0200 BJT derived from JRA-25. The lines perpendicular to the *x* axis are for reference.

midtroposphere, reflecting the role of the eastern plain as a valley. Except for vertical velocity, the 850-hPa southwesterly flow over the eastern plain strengthens during night. The southwesterly flow contributes to the formation of the low-level jet and transports the warm tropical water vapor to the eastern plain, providing a favorable environment to the rainfall systems over this area.

Similar to those in the western plain, dominant early-morning rainfall (Fig. 9a) and upward motion (gray solid lines in Fig. 10) exist in the East China Sea, which can be partly attributed to the large-scale "land–sea breezes." The early-morning diurnal peak can also be verified in some island stations in gauge data (Fig. 9b).

8. Summary and concluding remarks

Using rain gauge and TRMM 3B42 data, we demonstrated the regional diurnal features of precipitation, including the rainfall amount, frequency, and intensity over subtropical East Asia.

The gauge and TRMM 3B42 data exhibit generally consistent diurnal variations with significant regional features over subtropical East Asia. Four different regimes of diurnal variations have been identified. Over the Tibetan Plateau, the maximum rainfall occurs in the late afternoon and at midnight; in the western plain, the rainfall shows delayed phases from midnight to early morning; in the eastern plain, the major peak occurs in the late afternoon with a secondary early-morning peak that is obscured in 3B42; over the East China Sea, maximum rainfall occurs in the early morning. The diurnal features of rainfall amount and frequency are found to be more coherent than rainfall intensity. The late-afternoon peak in rainfall amount over the eastern plain is mainly contributed by the rainfall intensity, while the early-morning one is mainly attributed to the rainfall frequency.

Over the eastern and western plains, the correlation of diurnal variations of rainfall amount between 3B42 and Gdata is higher than that of frequency and intensity. In these two regions, the diurnal peak of rainfall frequency occurring in the early morning is underestimated and the

midnight and early-morning peaks of rainfall intensity are overestimated in 3B42, in comparison with those in Gdata.

The different diurnal features between the total rainfall amount over the land and the sea can be attributed to the distinct diurnal variations of convective rainfall over different underlying surfaces. The stratiform precipitation shows similar diurnal phases over the land and the sea. The propagating phases along the tropical coastlines are not observed in this subtropical ocean.

We have also found that diurnal phases are highly correlated with the underlying surfaces and the elevations. The characterizations of the diurnal rainfall variations over subtropical East Asia should not only improve our understanding of regional climate but also serve as valuable diagnostic metrics for the climate modeling community in evaluating model performances over East Asia.

REFERENCES

Aves, S. L., and R. H. Johnson, 2008: The diurnal cycle of convection over the northern South China Sea. *J. Meteor. Soc. Japan,* **86,** 919–934.

Betts, A. K., and C. Jakob, 2002: Evaluation of the diurnal cycle of precipitation, surface thermodynamics, and surface fluxes in the ECMWF model using LBA data. *J. Geophys. Res.,* **107,** 8045, doi:10.1029/2001JD000427.

Bleeker, W., and M. J. Andre, 1951: On the diurnal variation of precipitation, particularly over central U.S.A., and its relation to large-scale orographic circulation systems. *Quart. J. Roy. Meteor. Soc.,* **77,** 260–271.

Chen, G., W. Sha, and T. Iwasaki, 2009: Diurnal variation of precipitation over southeastern China: Spatial distribution and its seasonality. *J. Geophys. Res.,* **114,** D13103, doi:10.1029/2008JD011103.

Chen, G. T.-J., 1983: Observational aspects of the mei-yu phenomenon in sub-tropical China. *J. Meteor. Soc. Japan,* **61,** 306–312.

Chen, H., R. Yu, J. Li, W. Yuan, and T. Zhou, 2010: Why nocturnal long-duration rainfall presents an eastward-delayed diurnal phase of rainfall down the Yangtze River valley. *J. Climate,* **23,** 905–917.

——, W. Yuan, J. Li, and R. Yu, 2012: A possible cause for different diurnal variations of warm season rainfall as shown in station observations and TRMM 3B42 data over the southeastern Tibetan Plateau. *Adv. Atmos. Sci.,* **29,** 193–200.

Dai, A., and C. Deser, 1999: Diurnal and semidiurnal variations in global surface wind and divergence fields. *J. Geophys. Res.,* **104,** 31 109–31 125.

——, and K. E. Trenberth, 2004: The diurnal cycle and its depiction in the Community Climate System Model. *J. Climate,* **17,** 930–951.

——, X. Lin, and K.-L. Hsu, 2007: The frequency, intensity, and diurnal cycle of precipitation in surface and satellite observations over low- and mid-latitudes. *Climate Dyn.,* **29,** 727–744.

Ding, Y., 1992: Summer monsoon rainfalls in China. *J. Meteor. Soc. Japan,* **70,** 373–396.

Fujinami, H., S. Nomura, and T. Yasunari, 2005: Characteristics of diurnal variations in convection and precipitation over the southern Tibetan Plateau during summer. *SOLA,* **1,** 49–52.

He, H., and F. Zhang, 2010: Diurnal variations of warm-season precipitation over northern China. *Mon. Wea. Rev.,* **138,** 1017–1025.

Huang, A., Y. Zhang, and J. Zhu, 2008: Impacts of physical process parameterizations on simulation of the diurnal variations of summer precipitation over China (in Chinese). *Adv. Earth Sci.,* **23,** 1174–1184.

Huang, W.-R., J. C. L. Chan, and S.-Y. Wang, 2010: A planetary-scale land–sea breeze circulation in East Asia and the western North Pacific. *Quart. J. Roy. Meteor. Soc.,* **136,** 1543–1553.

Huffman, G. J., and Coauthors, 2007: The TRMM Multisatellite Precipitation Analysis (TMPA): Quasi-global, multiyear, combined-sensor precipitation estimates at fine scales. *J. Hydrometeor.,* **8,** 38–55.

Ichikawa, H., and T. Yasunari, 2006: Time–space characteristics of diurnal rainfall over Borneo and surrounding oceans as observed by TRMM-PR. *J. Climate,* **19,** 1238–1260.

Iguchi, T., T. Kozu, R. Meneghini, J. Awaka, and K. Okamoto, 2000: Rain-profiling algorithm for the TRMM precipitation radar. *J. Appl. Meteor.,* **39,** 2038–2052.

Johnson, R. H., Z. Wang, and J. F. Bresch, 1993: Heat and moisture budgets over China during the early summer monsoon. *J. Meteor. Soc. Japan,* **71,** 137–152.

Kidder, S. Q., and T. H. Vonder Haar, 1995: *Satellite Meteorology: An Introduction.* Academic Press, 466 pp.

Kikuchi, K., and B. Wang, 2008: Diurnal precipitation regimes in the global tropics. *J. Climate,* **21,** 2680–2696.

Li, J., R. Yu, T. Zhou, and B. Wang, 2005: Why is there an early spring cooling shift downstream of the Tibetan Plateau? *J. Climate,* **18,** 4660–4668.

——, ——, and ——, 2008: Seasonal variation of the diurnal cycle of rainfall in southern contiguous China. *J. Climate,* **21,** 6036–6043.

——, ——, W. Yuan, and H. Chen, 2011: Changes in duration-related characteristics of late-summer precipitation over eastern China in the past 40 years. *J. Climate,* **24,** 5683–5690.

Li, W., C. Luo, D. Wang, and T. Lei, 2010: Diurnal variations of precipitation over the South China Sea. *Meteor. Atmos. Phys.,* **109,** 33–46.

Lin, X., D. A. Randall, and L. D. Fowler, 2000: Diurnal variability of the hydrologic cycle and radiative fluxes: Comparisons between observations and a GCM. *J. Climate,* **13,** 4159–4179.

Liu, X., A. Bai, and C. Liu, 2009: Diurnal variations of summertime precipitation over the Tibetan Plateau in relation to orographically-induced regional circulations. *Environ. Res. Lett.,* **4,** 045203, doi:10.1088/1748-9326/4/4/045203.

Lu, J., 1942: Nocturnal precipitation in Bashan Mountain (in Chinese). *Acta Meteor. Sin.,* **16,** 36–53.

Lu, X., and H. Xu, 2007: Diurnal variations of rainfall in summer over the Indo-China Peninsula (in Chinese). *J. Nanjing Inst. Meteor.,* **30,** 632–642.

Masunaga, H., T. Iguchi, R. Oki, and M. Kachi, 2002: Comparison of rainfall products derived from TRMM Microwave Imager and precipitation radar. *J. Appl. Meteor.,* **41,** 849–862.

Ohsawa, T., H. Ueda, T. Hayashi, A. Watanabe, and J. Matsumoto, 2001: Diurnal variations of convective activity and rainfall in tropical Asia. *J. Meteor. Soc. Japan,* **79,** 333–352.

Onogi, K., and Coauthors, 2007: The JRA-25 Reanalysis. *J. Meteor. Soc. Japan,* **85,** 369–432.

Peng, G., F. Chai, Q. Zeng, and R. Yu, 1994: Research on ''Ya-An-Tian-Lou'' part I: Weather analysis (in Chinese). *Sci. Atmos. Sin.,* **18,** 466–475.

Ramage, C. S., 1952: Diurnal variation of summer rainfall over east China, Korea and Japan. *J. Meteor.,* **9,** 83–86.

Sanderson, V. L., C. Kidd, and G. R. McGregor, 2006: A comparison of TRMM microwave techniques for detecting the diurnal rainfall cycle. *J. Hydrometeor.,* **7,** 687–704.

Sapiano, M. R. P., and P. A. Arkin, 2009: An intercomparison and validation of high-resolution satellite precipitation estimates with 3-hourly gauge data. *J. Hydrometeor.,* **10,** 149–166.

Singh, P., and K. Nakamura, 2009: Diurnal variation in summer precipitation over the central Tibetan Plateau. *J. Geophys. Res.,* **114,** D20107, doi:10.1029/2009JD011788.

Sorooshian, S., X. Gao, K. Hsu, R. A. Maddox, Y. Hong, H. V. Gupta, and B. Imam, 2002: Diurnal variability of tropical rainfall retrieved from combined GOES and TRMM satellite information. *J. Climate,* **15,** 983–1001.

Tao, S. Y., and L. X. Chen, 1987: A review of recent research on the East Asian summer monsoon. *Monsoon Meteorology,* C. P. Chang and T. N. Krishnamurti, Eds., Oxford University Press, 60–92.

Todd, M., E. Barrett, M. Beaumont, and T. Bellerby, 1999: Estimation of daily rainfall over the Upper Nile River basin using a continuously calibrated satellite infrared technique. *Meteor. Appl.,* **6,** 201–210.

Trenberth, K. E., A. Dai, R. M. Rasmussen, and D. B. Parsons, 2003: The changing character of precipitation. *Bull. Amer. Meteor. Soc.,* **84,** 1205–1217.

Wang, C.-C., G. T.-J. Chen, and R. E. Carbone, 2004: A climatology of warm-season cloud patterns over East Asia based on GMS infrared brightness temperature observations. *Mon. Wea. Rev.,* **132,** 1606–1629.

Wang, D., and Y. Zhang, 2009: Diurnal variations of precipitation and circulation simulated by model for interdisciplinary research on climate (in Chinese). *J. Nanjing Univ.,* **45,** 724–733.

Wang, F., R. Yu, H. Chen, J. Li, and W. Yuan, 2011: The characteristics of rainfall diurnal variation over the southwestern China. *Torrential Rain Disasters,* **2,** 117–121.

Wu, G., and Coauthors, 2007: The influence of mechanical and thermal forcing by the Tibetan Plateau on Asian climate. *J. Hydrometeor.,* **8,** 770–789.

Xu, W., and E. J. Zipser, 2011: Diurnal variations of precipitation, deep convection, and lightning over and east of the eastern Tibetan Plateau. *J. Climate,* **24,** 448–465.

Yanai, M., and C. Li, 1994: Mechanism of heating and the boundary layer over the Tibetan Plateau. *Mon. Wea. Rev.,* **122,** 305–323.

Yang, G.-Y., and J. Slingo, 2001: The diurnal cycle in the tropics. *Mon. Wea. Rev.,* **129,** 784–801.

Yang, S., and E. A. Smith, 2006: Mechanisms for diurnal variability of global tropical rainfall observed from TRMM. *J. Climate,* **19,** 5190–5226.

Ye, D. Z., and Y. X. Gao, 1979: *Meteorology of Qinghai-Xizang (Tibet) Plateau*. Science Press, 278 pp.

Yeh, T.-C., S.-W. Luo, and P.-C. Chu, 1957: The wind structure and heat balance in the lower troposphere over Tibetan Plateau and its surrounding. *Acta Meteor. Sin.,* **28,** 108–121.

Yin, S., D. Chen, and Y. Xie, 2009: Diurnal variations of precipitation during the warm season over China. *Int. J. Climatol.,* **29,** 1154–1170.

Yu, R., B. Wang, and T. Zhou, 2004: Climate effects of the deep continental stratus clouds generated by the Tibetan Plateau. *J. Climate,* **17,** 2702–2713.

——, Y. Xu, T. Zhou, and J. Li, 2007a: Relation between rainfall duration and diurnal variation in the warm season precipitation over central eastern China. *Geophys. Res. Lett.,* **34,** L13703, doi:10.1029/2007GL030315.

——, T. Zhou, A. Xiong, Y. Zhu, and J. Li, 2007b: Diurnal variations of summer precipitation over contiguous China. *Geophys. Res. Lett.,* **34,** L01704, doi:10.1029/2006GL028129.

——, J. Li, and H. Chen, 2009: Diurnal variation of surface wind over central eastern China. *Climate Dyn.,* **33,** 1089–1097.

Yuan, W., R. Yu, H. Chen, J. Li, and M. Zhang, 2010: Subseasonal characteristics of diurnal variation in summer monsoon rainfall over central eastern China. *J. Climate,* **23,** 6684–6695.

——, J. Li, H. Chen, and R. Yu, 2012: Intercomparison of summer rainfall diurnal features between station rain gauge data and TRMM 3B42 product over central eastern China. *Int. J. Climatol.,* in press.

Zhao, Z., R. Leung, and Y. Qian, 2005: Characteristics of summer rainfall in China for the recent years (in Chinese). *Adv. Climate Change Res.,* **1,** 29–31.

Zhou, T., and R. Yu, 2005: Atmospheric water vapor transport associated with typical anomalous summer rainfall patterns in China. *J. Geophys. Res.,* **110,** D08104, doi:10.1029/2004JD005413.

——, ——, H. Chen, A. Dai, and Y. Pan, 2008: Summer precipitation frequency, intensity, and diurnal cycle over China: A comparison of satellite data with rain gauge observations. *J. Climate,* **21,** 3997–4010.